Dynamics of the semi-diurnal and quarter-diurnal internal tides in the Bay of Biscay. Part 2: Baroclinic tides

Ivane L. Pairaud [a,d,*], Francis Auclair [a], Patrick Marsaleix [a], Florent Lyard [b], Annick Pichon [c]

[a] Laboratoire d'Aérologie, CNRS et Université de Toulouse, Observatoire Midi-Pyrénées, 14 av. Edouard Belin, 31400 Toulouse, France
[b] LEGOS, CNRS et Université de Toulouse, Observatoire Midi-Pyrénées, 18 av. Edouard Belin, 31400 Toulouse, France
[c] Service Hydrographique et Océanographique de la Marine, Centre Militaire d'Océanographie, 13 rue le Chatellier, BP 30316, 29603 Brest Cedex, France
[d] IFREMER, Laboratoire Provence Azur Corse, BP 330, 83507, La Seyne sur Mer Cedex, France

ARTICLE INFO

ABSTRACT

A regional baroclinic model forced with several tidal constituents at different frequencies is used to investigate the internal tide of the Bay of Biscay. The regional ocean model is free surface, sigma-coordinate and it is implemented in order to accurately take into account the barotropic forcing, the strong bathymetry gradients and the temperature and salinity stratifications. In a previous paper, the barotropic component of the tides was studied in details and the boundary conditions of the three-dimensional model were extracted from the atlases. In the present paper, we focus on the baroclinic component of the tides and the simulations are validated against observations from the MINT94 experiment. The observed currents and stratification are accurately reproduced by the model. The internal tide pattern is consistent with the descriptions found in the literature. Combining wavelet and principal component analysis we extract the patterns of generation and propagation of the internal tide at the semi-diurnal and quarter-diurnal frequencies. Secondary internal wave generation areas are identified over the plain. The vertical displacements of isopycnal surfaces for the M4 internal tide are found to be locally half those induced by the semi-diurnal internal tide. A sensitivity study shows the impact of using a three-dimensional initial stratification over the direction of propagation and wavelengths of the internal tides.

1. Introduction

Research dealing with the origin of the ocean dyapicnal mixing has been given a renewed interest in the recent years since this mixing appeared to control, at least partially, the ocean stratification, the meridional oceanic circulation, heat transports and the climate response (Saenko, 2006). Among other processes, internal waves are thought to be a major contributor to the mechanical energy which is necessary for the ocean mixing (Munk and Wunsch, 1998; Garrett and St Laurent, 2002; St Laurent and Garrett, 2002; Wunsch and Ferrari, 2004). Internal waves are created by the action of the wind over the surface layer and by the interaction of the tide with the bathymetry. They feed the mixing by breaking or leading to direct instability and turbulence in the deep ocean. The energetic content of both energy sources may be roughly estimated at global scale and is likely to be comparable: the most recent estimates are between 1 and 1.5 TW for the wind and about 1 TW for the tide (Wunsch and Ferrari, 2004). Through the associated mixing, the internal tide can have a non-negligible impact over sediment transport (Cacchione and Drake, 1986) and biological growth in specific sites of the ocean (Pingree and Mardell, 1981).

A review of previous studies dealing with the internal tide in the deep-ocean can be found in Garrett and Kunze (2007). In the Hawaii Ocean-Mixing Experiment (HOME), researchers from different institutions have shared their knowledge of observations and modeling in order to quantify the tidal energy transfers over the Hawaiian ridge (Pinkle and Rudnick, 2006). It has been found that 20 GW of barotropic tidal energy were dissipated along the Hawaiian Island chain in specific sites (2% of the 1 TW global pelagic tidal dissipation) (Egbert and Ray, 2001). The generation of the internal tide is enhanced by three major forcings: a strong barotropic tidal forcing, a steep slope of the sea-floor (such as at ridges and shelf breaks) and strong stratification gradients (thermoclines). When the barotropic tidal velocity remains significantly less than the phase speed of the generated internal tide, then the linear theory prevails (otherwise higher harmonics can develop) (Vlasenko et al., 2005). Barotropic tides above steep

* Corresponding author at: IFREMER, Laboratoire Provence Azur Corse, BP 330, 83507, La Seyne sur Mer Cedex, France.
E-mail addresses: ivane.pairaud@ifremer.fr (I.L. Pairaud), francis.auclair@aero.obs-mip.fr (F. Auclair), patrick.marsaleix@aero.obs-mip.fr (P. Marsaleix), florent.lyard@legos.obs-mip.fr (F. Lyard), pichon@shom.fr (A. Pichon).

topography give birth to internal tides at critical slopes, the regions where the direction of the wave beam is tangent to the slope of the topography (Baines, 1982). A large number of baroclinic tidal modes are generated, which combine into beams or ray of internal tidal energy (New, 1988). The generation of the internal tide at a continental slope has been reproduced in laboratory experiments by Gostiaux and Dauxois (2007). They also reproduced the beam-like propagation of the internal tide. Strong non-linear effects and mixing can be found in the generation region itself. In regions where the beam reflects (bottom, surface), ingoing and outgoing beams interact inducing non-linear advection of overlapping internal wave beams, as shown by the numerical work of Gerkema et al. (2006) and the experimental work of Peacock and Tabaei (2005) and Gostiaux et al. (2006).

In the Bay of Biscay, the internal tide is mainly semi-diurnal (Pingree and New, 1989) due to the dominance of the semi-diurnal M2 barotropic forcing above the shelf break. Two main generation area have been identified: the Northern shelf break near La Chapelle bank (New and Pingree, 1990; Pichon and Correard, 2006) and the Cape Finisterre region off Northwest Spain (Pichon and Correard, 2006; Azevedo et al., 2006). The beams have been observed to emanate from the upper part of the continental slope where it becomes critical (Pingree and New, 1991; Jezequel et al., 2002). The characteristics of the internal tide can be inferred from observations and model predictions through some disturbances induced by the internal waves in the oceanic density and velocity structure at the tidal frequency. Large amplitude internal tide beams were first reported from in situ observations in the Bay of Biscay by Pingree and New (1989), with values ranging from about 150 m near the upper slopes to 100 m farther out. Pingree and New (1989) have also highlighted the spatial variability in the internal tide, with a reduction of the amplitude and a spreading of the beam during the propagation from the shelf break. The wavelength associated with the propagation of the internal tide varies with the stratification. It was estimated from the sea surface signature of the vertical motion induced by the internal tide. From remotely sensed AVHRR "sunglint" imagery in the visible band (Pingree and New, 1995) and SAR imagery (New and Da Silva, 2002), values of 30–35 km were found onto the shelf in summer, against 40–50 km for the oceanward tides. The SAR images of New and Da Silva (2002) also showed that the ray that propagates downwards from the Northern shelf break reflects from the sea bottom and resurfaces some 150 km away from the shelf break. The Bay of Biscay thus shows a complex pattern with several area of internal tide generation, several directions of propagation of the waves, at different frequencies. A joint approach combining observations at sea, theoretical basis and numerical models is required. The numerical model is the only way to complete the observations in order to have a simultaneous and synoptic view of all the parameters, but it has to be set up and validated using observations.

Until recent years, nearly all tidal studies using numerical models were dedicated to the M2 internal tide. In the past decades, the models were first based on simple academic approaches and they were restricted to idealized topography in the coastal zone. Several authors have proposed analytical solutions for the generation of the internal tide by interaction of the tidal flow over topography (Garrett and Kunze, 2007), based on the ray tracing theory or the decomposition over normal modes (e.g. Rattray, 1960; Cox and Sandstrom, 1962; Baines, 1973, 1974; Bell, 1975; Prinsenberg and Rattray, 1975). These models, which are linear in the dynamics, led to other developments that give analytical expressions for the rate at which energy is input to the internal wave field (Craig, 1987; Llewellyn Smith and Young, 2002; Khatiwala, 2003). In the case of internal tides

generated at shelf slopes at M2 frequency, the two-dimensional analytical model of Baines (1982), namely the body force approach, gives the energy conversion from barotropic to baroclinic tides. One of the most important energy conversion rate was found to be located at the continental shelf slope of the North Atlantic ocean centered around the Bay of Biscay and the English Channel. But there are a lot of oceanic regions in which simple analytic models cannot be used any more, as in the case of a corrugated continental slope (Legg, 2004). In order to study the influence of the variations in the stratification and bathymetry over the internal tidal field, taking into account the presence of rotation and non-linearity, numerical models have been implemented. Numerical two-dimensional models have been used in order to estimate the semi-diurnal tidal offshore energy flux in regions such as the Australian northwest shelf (Holloway, 1996; Xing and Davies, 1997). However, Munk and Wunsch (1998) have shown that the two-dimensional hypothesis in the theory by Baines (1982) is too restrictive and that three-dimensional features are likely to contribute significantly. Various studies using three-dimensional models were performed showing the influence of the barotropic forcing, the stratification and the shape of the topography on the characteristics of the internal tide in a wide range of geographical locations (Cummins and Oey, 1997; Xing and Davies, 1999; Robertson, 2001; Merrifield and Holloway, 2002; Niwa and Toshiyuki, 2004; Simmons et al., 2004; Hibiya, 2004; Munroe and Lamb, 2005). In particular, Pichon and Correard (2006) applied the three-dimensional isopycnal model MICOM to the study of the internal tide in the Bay of Biscay, focusing on the continental slope and abyssal plain (i.e. they did not model the shelf). The initial stratification was chosen horizontally homogeneous, as in a number of internal tide modeling studies (for example in Gerkema et al., 2004). The tidal forcing was restricted to the use of semi-diurnal tidal solutions from a spectral model (Lyard and Le Provost, 1997), thus neglecting the quarter-diurnal and diurnal components of the tide. The internal tide obtained with MICOM was validated against observations from the MINT94 internal tide experiment performed by the SHOM (the French hydrographic and oceanographic naval service) in September and October 1994. This study showed the capacity to approach the complexity of the beam-like propagation of the internal tide in the deep part of the Bay of Biscay with an isopycnal model. The use of isopycnal coordinates in an adiabatic way (without coupling with the mixing model) gave the opportunity to keep the stratification close to an average realistic measured profile and to focus on the vertical displacement of isopycnics (amplitude of the internal tide), but neglecting local spatial variations in the stratification due for instance to an enhanced mixing by internal tides.

In this paper, the aim is to qualify and quantify numerically the mechanisms of generation and propagation of internal tides in the abyssal plain, continental slope and shelf of the Bay of Biscay. This is achieved by using the three-dimensional regional SYMPHONIE model (Marsaleix et al., 2008). This model is particularly well adapted to the study of internal tides since it is energy conservative (Marsaleix et al., 2008) and as a consequence it does not suffer any spurious energy loss when representing energy transfers. The model uses a realistic bathymetry, which is enhanced by the use of a high horizontal resolution and generalized sigma coordinates in the vertical. A particular attention was paid to the modeling of the barotropic tide, as it is one of the three main forcings for the generation of internal tides. In a previous paper (Pairaud et al., 2008), a two-dimensional high resolution configuration of the SYMPHONIE model was embedded into the T-UGOm tidal model of the North-East Atlantic. We showed that a large amount of energy was to be transferred from the surface tide (mostly M2) to the internal tide at the semi-diurnal frequency over the shelf break, with a maximum located in southern French Brittany near La Chapelle bank (see the wave drag on Fig. 7 by Pairaud et al., 2008). The three-dimensional model is forced by

multi-frequency tidal solutions including semi-diurnal, diurnal and quarter-diurnal components that were validated against observations. It is, to the best of our knowledge, the first study of internal tide which takes into account an accurate barotropic forcing by the quarter-diurnal tide M4 in the Bay of Biscay. The prescribed stratification is first taken horizontally homogeneous, but we investigate the influence of choosing a three-dimensional initial stratification on the modeled internal tides by using a POP 3D stratification (B. Levier, pers. comm.). As was done for the surface tide in a previous paper (Pairaud et al., 2008), both the semi-diurnal and the non-linear quarter-diurnal M4 internal tide are investigated through the WEof analysis, i.e. wavelet empirical orthogonal function analysis (Pairaud and Auclair, 2005). This method allows for the investigation of the various scales involved when crossing the shelf break as well as the transitory dynamics of the waves.

This paper is organized as follows. The model configuration is presented in Section 2. In Section 3, we describe the characteristics of internal tides obtained with the model and their validation against observations from the MINT94 experiment. We discuss the characteristics of the semi-diurnal and quarter-diurnal internal tides that have emerged from the WEof analysis in Section 4. The influence of using a three-dimensional initial stratification over the internal tide is examined in Section 5. Finally, the results are summarized and discussed in Section 6.

2. The SYMPHONIE model configurations

We use the free surface, three-dimensional SYMPHONIE coastal ocean model described in detail by Marsaleix et al. (2006, 2008). It is based on the primitive equations and classical Boussinesq and hydrostatic pressure assumptions. The model has been applied to the study of internal gravity waves by Pairaud and Auclair (2005) and to the study of barotropic tides in the Bay of Biscay by Pairaud et al. (2008).

2.1. Model description

The three components of the current, sea surface elevation, temperature and salinity are computed on a C grid using a finite difference method (Arakawa and Lamb, 1977). High frequency barotropic processes and fast moving surface waves are explicitly solved. This exerts quite a strong CFL constraint on the model time stepping scheme but a time splitting technique (Blumberg and Mellor, 1987) allows to compute the vertical shear of the horizontal current and the depth-averaged horizontal components separately with appropriate time steps. Bottom friction is computed through a logarithmic parameterization of the bottom boundary layer. The simulations of the Bay of Biscay (Fig. 1) use a horizontal resolution of 1.5 km (see Table 1 for details). As the generation of internal waves is known to depend on the slope of the shelf break, a generalized sigma coordinate transformation is used in order to have an accurate representation of the bottom boundary condition. Simultaneously, this coordinate allows to accurately represent the surface layer marked by a strong seasonal thermocline influencing the internal tides in the Bay of Biscay. The generalized sigma coordinate used in the SYMPHONIE model has been described in details by Ulses et al. (2008, pp. 4–7). The vertical resolution becomes close to a constant value near the surface and bottom, whereas it is close to the standard sigma increment at a chosen depth between.

In order to deal with the well known problem of pressure truncation errors associated with the use of sigma coordinates, we use the results of the study by Auclair et al. (2000b) and a light
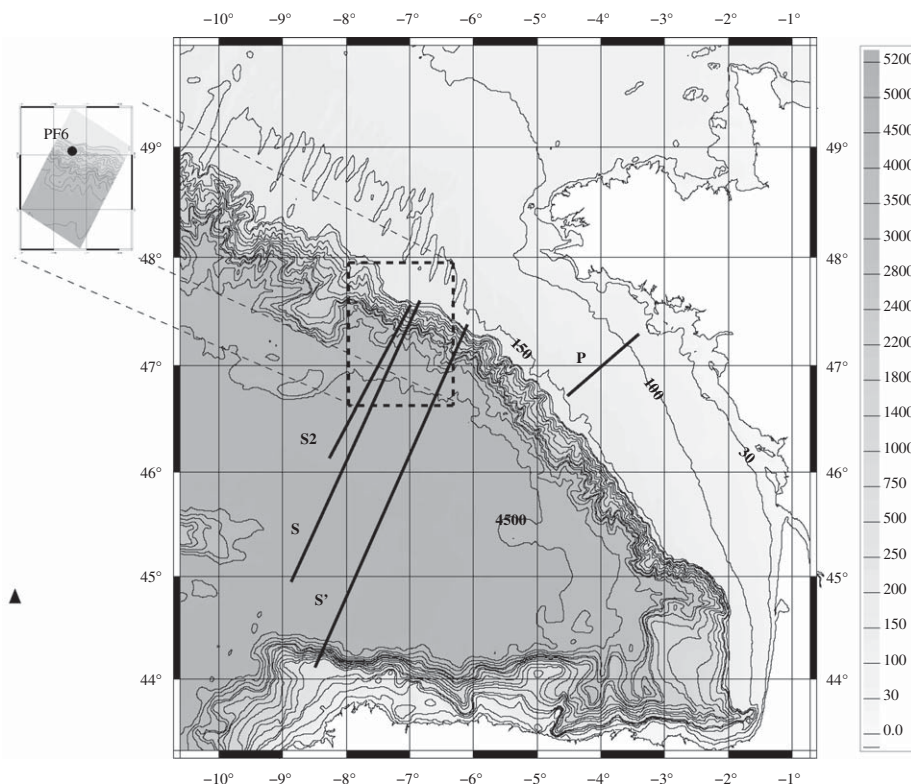

Fig. 1. Bathymetry of the model domain for the study of internal tides (depths in meters) and location of radials S2 [(46.25N,8.23W),(47.6N,7W)], S [(44.9N,8.9W),(47.5N,6.9W)], S′ [(44.17N,8.59W),(47.37N,6.05W)] and P [(46.7N,4.5W),(47.3N,3.4W)]. A zoom over the slope shows the PF6 station measurement (47.47N, 7.18W).

Table 1
Modeling characteristics for the internal tide experiment.

	Exp HR
Number of horizontal points along x	502
Number of horizontal points along y	490
Horizontal grid resolution (km)	1.5
Number of vertical levels	46
External time step (s)	2.1
Internal time step (s)	27.9
Horizontal diffusivity ($m^2 s^{-1}$)	7.5

The number of grid points and the horizontal grid resolution are given together with the external and internal time steps and the imposed horizontal viscosity coefficient.

smoothing is applied to the bathymetry. Following the method by Beckmann and Haidvogel (1993), we impose the constraint for the "slope parameter" in both directions of space given by $\Delta h / 2\bar{h} < 1$ where $\bar{h}$ is the mean depth between two adjacent points. The spurious geostrophic currents induced by the truncation error are maximum above the slope where the density stratification is large, but a special attention is paid to the reduction of those errors in the model (Auclair et al., 2000b; Marsaleix et al., 2008).

The internal tide is very sensitive to the parameterization of mixing in the model as the stratification is likely to be eroded in case of overestimated mixing. In this study, viscosity coefficients related to horizontal fluxes are taken to be constant in time but dependent on the size of horizontal grid. Viscosity and diffusivity coefficients related to vertical fluxes are calculated according to Gaspar et al. (1990) second-order closure scheme for the momentum, with a prognostic equation for the turbulent kinetic energy and an algebraic formulation of the mixing and dissipation lengths. The vertical diffusivity for temperature and salinity is made of two components. We first introduce a low diffusivity coefficient equal to 10^{-6} $m^2 s^{-1}$ in the turbulent closure scheme, in order to avoid an erosion of the stratification.

The second component of the diffusivity is introduced in the advection scheme which is a centered scheme with an additional upstream component (Marsaleix et al., 2008).

The present modeling study of the MINT94 experiment over the Bay of Biscay has been designed to provide further information with respect to the study by Pichon and Correard (2006) which is based on the isopycnal model MICOM, i.e. on rather different modeling strategies and assumptions. It first provides an original comparison of σ and isopycnal coordinate models in the context of the realistic modeling of internal tides. The isopycnal study being inviscid, we thus have an opportunity to evaluate the diffusive properties (whether physical or numerical) of the free surface σ- coordinate time splitting regional ocean model. To this respect, the chosen model is energy conservative, which means in particular that the numerical energy transfers are equilibrated and controlled as carefully demonstrated by Marsaleix et al. (2008). Pichon and Correard (2006) did not have the opportunity to model the evolution of the mixing layer nor the propagation of the internal tides over the shelf. This can be finally achieved in the present study, offering an interesting extension of the previous results in this region. The tidal forcing is also generalized to the nine largest tidal waves, offering an original opportunity to quantify the quarter-diurnal (M4) internal tide.

2.2. Model forcing

Special attention was paid to the open boundary conditions (OBC) since spurious reflections of outgoing waves at open boundaries can have a significant impact on the inner domain solution. The time scales associated with the propagation of
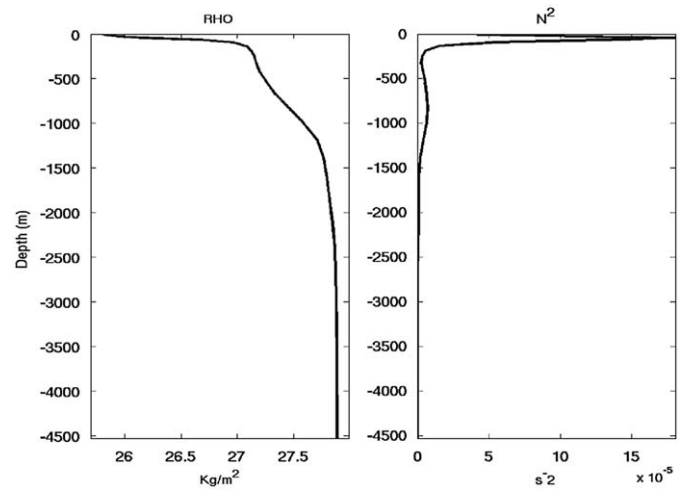

Fig. 2. Density profile from the MINT94 experiment and associated Brunt–Väisälä frequency for the month of September used to initialize the model stratification. The average profile has been obtained by Pichon and Correard (2006) using CTD and ADCP data (250 profiles) from the campaign for the 2500 first meters. For the deeper layer the density comes from a mean annual profile from the SHOM hydrologic database. This profile is characterized by the presence of a permanent pycnocline in the intermediate layer and a seasonal thermocline in the upper layer.

waves throughout the Bay of Biscay area (about 1.1 h for a barotropic semi-diurnal wave and 42 h for the related internal wave generated at the continental slope) is much shorter than the length of our simulations (17 days). The radiative boundary conditions (Flather, 1976) are used for the tidal barotropic field whereas boundary baroclinic currents and tracers are prescribed through a classical *Sommerfeld* condition. Details of the numerical implementation of the OBC are given in Marsaleix et al. (2006).

The barotropic tidal forcing is described in Pairaud et al. (2008). It includes tidal elevations and barotropic currents for nine components (semi-diurnal, diurnal and quarter-diurnal tides) given by the NEA-2004 atlas: M2, S2, N2, K2, K1, O1, P1 Q1 and M4. In addition, tidal forcing includes the tidal potential due to astronomical effects and loading and self-attraction effects (see their Appendix A, p. 1315).

A mean one-dimensional vertical profile inferred from the MINT94 experiment measurements (Pichon and Correard, 2006) is used as the background density field (Fig. 2). This is the first step toward the full understanding of the internal tide dynamics of the area, as an influence of three-dimensional variations in temperature can be expected in the Bay of Biscay (van Aken, 2000). The influence of using a three-dimensional initial density profile on the propagation of internal tides will be discussed further in Section 5.

3. Baroclinic tides in the Bay of Biscay

In the following, the main characteristics of the internal waves in the Bay of Biscay are obtained from the basic wave theory. Model results are then discussed over radials P, S, S′ and S2 perpendicular to the slope and at the station PF6 shown in Fig. 1 (using maps of velocity and density profiles). The radials S, S′ and S2 are located over the abyssal plain whereas the radial P is located over the continental shelf. The radials S and S2 enable the study of the propagation from the region around La Chapelle bank. The radial S′ was chosen because internal tides generated by opposite slopes can interfere, giving birth to internal tides of large amplitude. The station PF6 is at the position (47.47N,7.18W) near the top of the slope on Section S2, at a depth of 1100 m. The radial

S2 and the station PF6 are introduced in order to make a comparison with the modeling results and observations from the MINT94 experiment (Pichon and Correard, 2006).

3.1. Propagation of internal tides: theoretical considerations

Internal wave energy propagates as beams along characteristic ray paths characterized by large amplitude oscillations (see for example Mowbray and Rarity, 1967; Pingree and New, 1989, 1991). In the WKB approximation, for little variations of the Brunt–Väisälä frequency N with depth z, the characteristic ray paths have a slope $\alpha(z)$ to the horizontal given by

$$\alpha(z) = \pm \left(\frac{\omega^2 - f^2}{N(z)^2 - \omega^2} \right)^{1/2} \tag{1}$$

In Eq. (1), $\omega = 2\pi/T$ is the pulsation and f is the Coriolis parameter. Over the shelf and in the upper part of the water column above the plain, the density field is nearly horizontally homogeneous (i.e. N is small). A local slope can be computed at any depth, as done by Pingree and New (1991, Fig. 9). The slope of the beam at M2 frequency makes an angle of about $\pi/2$ with the horizontal in these area and the internal tide does not exhibit a beamlike propagation. Deeper in the ocean, ray paths can be identified, which become more vertical near the sea floor.

Another description of internal tides is in terms of decomposition over normal modes (Gill, 1982; Pingree and New, 1991). "Long" internal gravity waves are then considered and the wave propagation can be expressed as a sum of normal modes (when assuming a flat bathymetry, that is over the shelf or over the abyssal plain). In the linear theory, the modes are obtained by solving the Taylor–Goldstein equation:

$$\frac{d^2 W_j}{dz^2} + k_{H,j}^2 \frac{N^2(z) - \omega^2}{\omega^2 - f^2} W_j = 0 \tag{2}$$

with

$$w_j = W_j(z) e^{i(\overrightarrow{k_{H,j}} \cdot \overrightarrow{x} - \omega t)} \tag{3}$$

where w_j is the vertical velocity of mode j, W_j its vertically varying amplitude and $\overrightarrow{k_{H,j}}$ the related horizontal wave vector.

The theoretical values for wavelengths and phase speeds for horizontally propagating modes at M2 and M4 frequencies can be obtained in the Bay of Biscay and are given in Table 2 for typical locations over the plain and over the shelf, using the MINT94 September stratification. The computation of the amplitudes of the baroclinic modes shown in Fig. 3 indicates that the first mode is maximum near 1250 m depth whereas the third mode has a first maximum near 70 m. The third mode can be dominant near the surface.

Table 2
Table of the propagation characteristics of internal tides for the semi-diurnal (M2) and quarter-diurnal (M4) component using the MINT94 stratification profile (Fig. 2).

Wave period	M2 $T = 12.4h$	M4 $T = 6.2h$
Abyssal plain (5000 m)		
λ_H (km)		
Mode 1	141	49
Mode 2	75	26
Mode 3	52	17
c_H (m s^{-1})		
Mode 1	3.2	2.2
Mode 2	1.7	1.2
Mode 3	1.2	0.8
Shelf (140 m)		
λ_H (km)		
Mode 1	33	12
Mode 2	13	5
Mode 3	9	3
c_H (m s^{-1})		
Mode 1	0.7	0.5
Mode 2	0.3	0.2
Mode 3	0.2	0.1

The horizontal wavelengths λ_H and the horizontal phase speeds c_H are given for the first three modes over the abyssal plain (depth of 5000 m) and over the continental shelf (depth of 140 m).
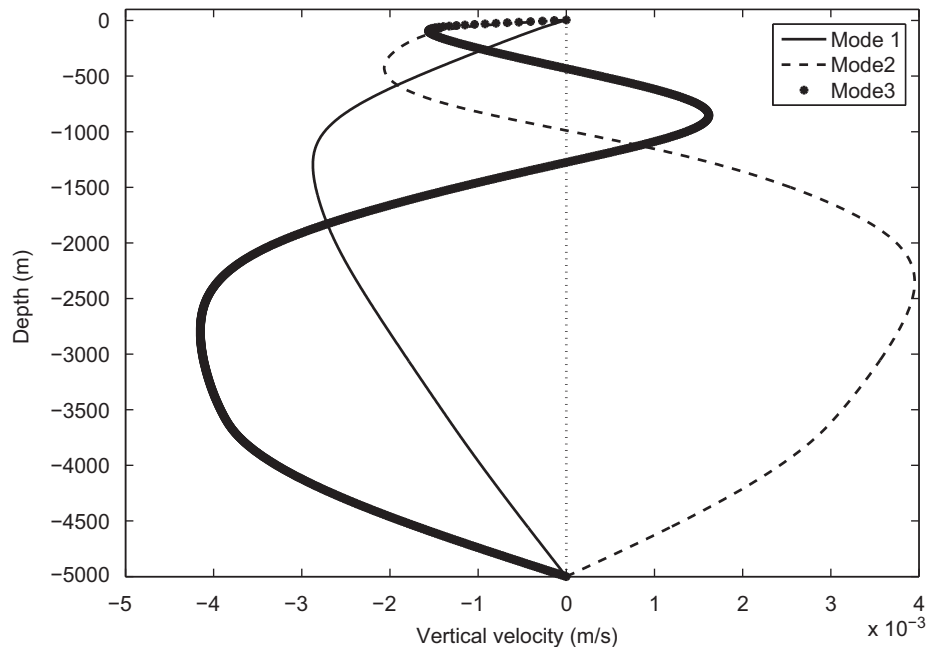

Fig. 3. First three baroclinic modes obtained by solving the Sturm–Liouville problem (Eq. (2)) for the Brunt–Väisälä frequency profile shown in Fig. 2. Amplitudes of the vertical velocity (m s^{-1}) are arbitrary since no normalization is applied for the different modes.

3.2. Global pattern of the internal tide over the bay

In this study, the choice has been made to consider an observed horizontally homogeneous stratification profile. It is based on an averaged profile (both in space and time) that includes the integrated effects of the wind, river discharges, mixing by the internal tide, etc. It includes the mixing layer as well as the thermoclines which are located at an average position along the water column. The use of this profile allows us to study the basic characteristics of the internal tide in the Bay of Biscay.

A pattern of the propagation of internal tides is presented in Fig. 4 using vertical velocity map (frame a) and horizontal velocity maps (frames b and c). The horizontal section in the seasonal thermocline (Fig. 4 a) exhibits internal waves propagating from the slope towards the abyssal plain and towards the coast. The most energetic propagation appears above the plain with higher vertical velocities. Horizontal wavelengths can be determined by an objective measurement from the horizontal and vertical velocity plots as the average distance between two wave crests or troughs (see Pairaud and Auclair, 2005, Appendix B for details). In accordance with the stratification and the depth, wavelengths are shorter above the shelf than above the plain (Table 2). Because of the local shape of the slope and the change in the shelf break orientation near La Chapelle bank, the internal wave is not seen to propagate similarly from all the locations along the continental slope. This results in stripes of vertical velocity maxima that are globally parallel to the shelf break but can be curved locally. This complex pattern may be reinforced by wave–wave interactions at
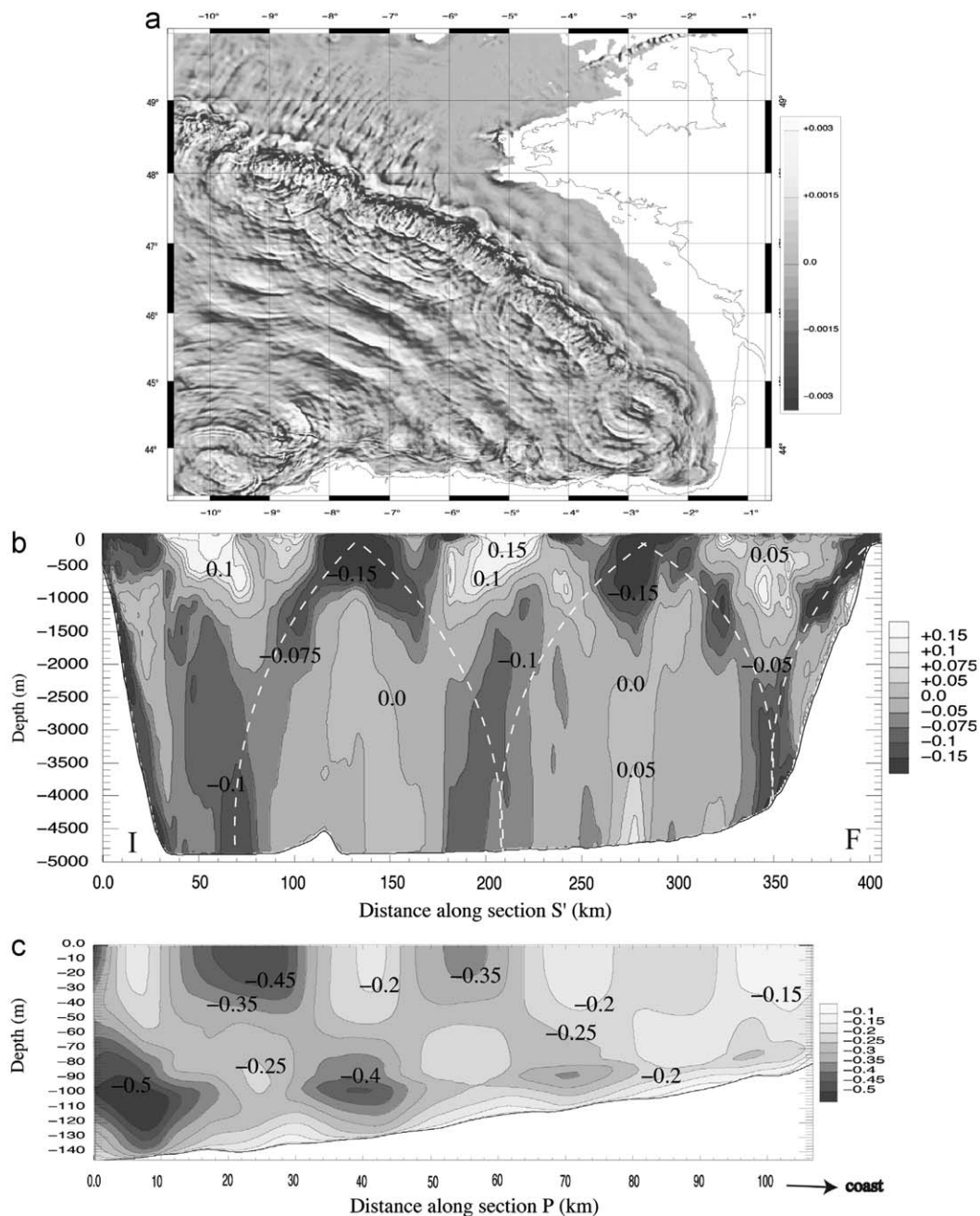

Fig. 4. Velocity sections for 9/09 1994 at 9:00 pm (m s^{-1}): (a) horizontal section of vertical velocity at 70 m deep, (b) total longitudinal horizontal velocity section along S′ (F and I correspond to the French and Iberian side of the section, respectively) over the abyssal plain with bold dashed lines representing the paths of the characteristic rays and (c) total longitudinal horizontal velocity section along P over the continental shelf.

various frequencies. There are three favored radials for the propagation of the internal tide perpendicular to the continental slope, as seen in Fig. 4 a. The most important propagation radial in terms of vertical velocities, and thus of amplitude of the internal tide, is the radial S′ arising from La Chapelle bank. This is consistent with the maximum generation area found by Pairaud et al. (2008) and with the observations in the Bay of Biscay (see also Pingree and New, 1995). Internal tides also propagate over the continental shelf, but are largely affected by the presence of the barotropic tides in this region. This results in an advection of the baroclinic tides by barotropic currents, which are much larger over the shelf than over the deep ocean (Pairaud et al., 2008). The additional dissipation due to the combination of barotropic and baroclinic currents in the presence of quadratic bottom friction implies a more rapid decrease of the amplitude of the internal tide, as was previously observed by Pingree et al. (1986).

From Fig. 4 a, horizontal wavelengths above the plain in the seasonal thermocline are of $\lambda_H = 47.6 \pm 4$ km after 13.9 days. From Table 2, this value is close to the theoretical value for a propagation dominated by the third baroclinic mode (with $\lambda_{H3,th} = 52$ km). As a comparison, observed values near the surface in the area for the month of September were of 45–50 km in the study by New and Da Silva (2002) from SAR images and Pingree and New (1995) obtained a value of about 46 km from a sunglint image.

Fig. 4 b shows the longitudinal velocity above the abyssal plain along Section S′ (i.e. the total velocity magnitude in the direction of the section). From this figure, the largest amplitudes of the velocity are located along beams and the velocity increases in the upper part of the water column above the main thermocline. The direction of the beam becomes steeper in the deeper part of the ocean, a manifestation of refraction effects. Besides, when reflecting at the sloping bottom, the beam defocuses, therefore

reducing the amplitude of the internal tide (Gerkema et al., 2004). The maxima of current are localized where the slope becomes critical (i.e. where the propagation angle of the beam equals the slope of the topography). Therefore a good representation of the bathymetry is crucial in order to accurately resolve the localization of the maxima and areas of reflection. From Fig. 4 b, the horizontal wavelength is $\lambda_H = 145 \pm 8$ km, except at the surface where it is three times less (as pointed out in Fig. 4 a). From Table 2, this value is close to the theoretical value for a propagation dominated by the first baroclinic mode (with $\lambda_{H1,th} = 141$ km). This is consistent with observations of the surface signature of the reflection of the main beam at the thermocline. This has been found to occur at approximately 140 km from the shelf break by New and Pingree (1990) and New and Da Silva (2002).

Fig. 4 c shows the longitudinal velocity above the shelf along Section P. There is a vertical shear in the vertical velocities. The horizontal wavelength obtained from this figure is $\lambda_{Hshelf} = 33.7 \pm 3$ km, which is close to the theoretical value for Mode 1 in Table 2 with $\lambda_{Hshelf,1th} = 33$ km.

From these results, one may conclude that the overall propagation pattern of the internal tide resulting from our simulation is close to what was observed in the previous studies.

3.3. Internal tide along Section S2

This subsection is dedicated to the propagation of the internal tide along the Section S2. This vertical section had been studied by Pichon and Correard (2006). Fig. 5 shows the longitudinal horizontal velocity (frame a) and the amplitude (frame b) of the semi-diurnal internal tide along Section S2. This is one of the most energetic radials in this region.
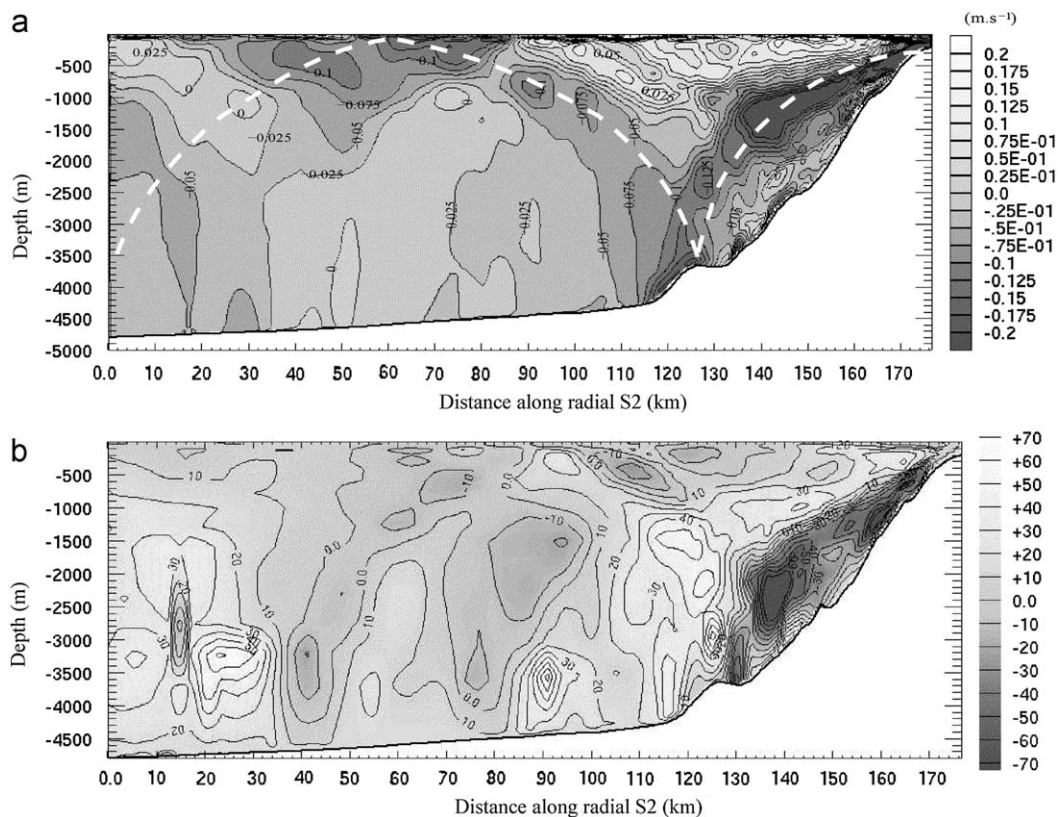

Fig. 5. (a) Total longitudinal horizontal velocity (m s⁻¹) along section S2 for 9/09 1994 at 9:00 pm with bold dashed lines representing the paths of the characteristic rays and (b) vertical displacement (m) of isopycnal surfaces for the semi-diurnal component of the internal tide for 9/09 at 9:00 pm.

From Fig. 5 a, the velocities over the plain are stronger near the shelf break close to the generation area. Above the plain, the horizontal velocity is stronger near the surface, in the seasonal thermocline, where it reaches more than $20\,cm\,s^{-1}$, while it is typically less than $2.5\,cm\,s^{-1}$ in the deep ocean. A plot of phases (not shown here) indicates that the internal tide at the end of the section is not in phase with the shelf break due to the presence of the spring-neap tidal cycle and the time needed by the internal wave to propagate, as pointed out by Pichon and Correard (2006). The amplitude of the internal tides is affected by the spring-neap cycle, by the multi-frequency nature of the forcing and by the presence of viscous effects which damp their amplitude during the propagation.

As the mean position of the isopycnal surfaces may evolve in time, a method based on wavelet analysis has been developed in order to get the vertical displacement with a mean position that changes during the experiment, as described in Appendix A. Fig. 5 b shows the (semi-diurnal) vertical displacement of the isopycnal surfaces with respect to their position at rest along Section S2 after 13 days. The wavelet based method gives a maximum vertical displacement near the generation area along the propagation beam. Maximum oscillations are spread over the deeper part of the water column where the stratification is weak, allowing for large vertical motions. The amplitude of the internal tide is less than $20\,m$ near the surface and can be more than $60\,m$ deeper in the ocean. This value is less than the $90\,m$ found by Pichon and Correard (2006, Fig. 9). A part of the explanation lies in the

introduction of the mixing associated with the propagation of the internal tide in the present study. The maximum vertical displacement can reach $200\,m$ after spring tide before the reflection of the beam at the bottom. In Fig. 5 b the amplitude of the vertical displacement is about $100\,m$ at $2600\,m$ depth and at a distance of 30–$35\,km$ from the generation area, whereas it is about $50\,m$ at the generation area. It is surprising that a maximum lies away from the generation area, since many observations, as highlighted for instance by Pingree and New (1989), have stated that the amplitude was reduced during the propagation. As the topography is made of about three steps so that the slope is far from uniform, more than one generation area can be found in depth, with a probable one around a depth of $3000\,m$. The internal tides propagating from the secondary generation areas can interfere constructively with the main beam and lead to larger oscillations.

Before its first reflection, the main beam is broad with a vertical extent of more than $1\,km$. The reflection of the beam occurs at about $45 \pm 10\,km$ from the generation area at a depth of $3700\,m$. These properties are comparable to the ones observed for an internal tide propagating from a southern part of the slope by Pingree and New (1991), who found that the reflection occurred at a depth of $4200\,m$, at approximately $50\,km$ from the upper slope. Differences in the shape of the slope in the two cases (the deeper step is more marked and a little shallower on radial S2) may explain the departure of the model from the observations.
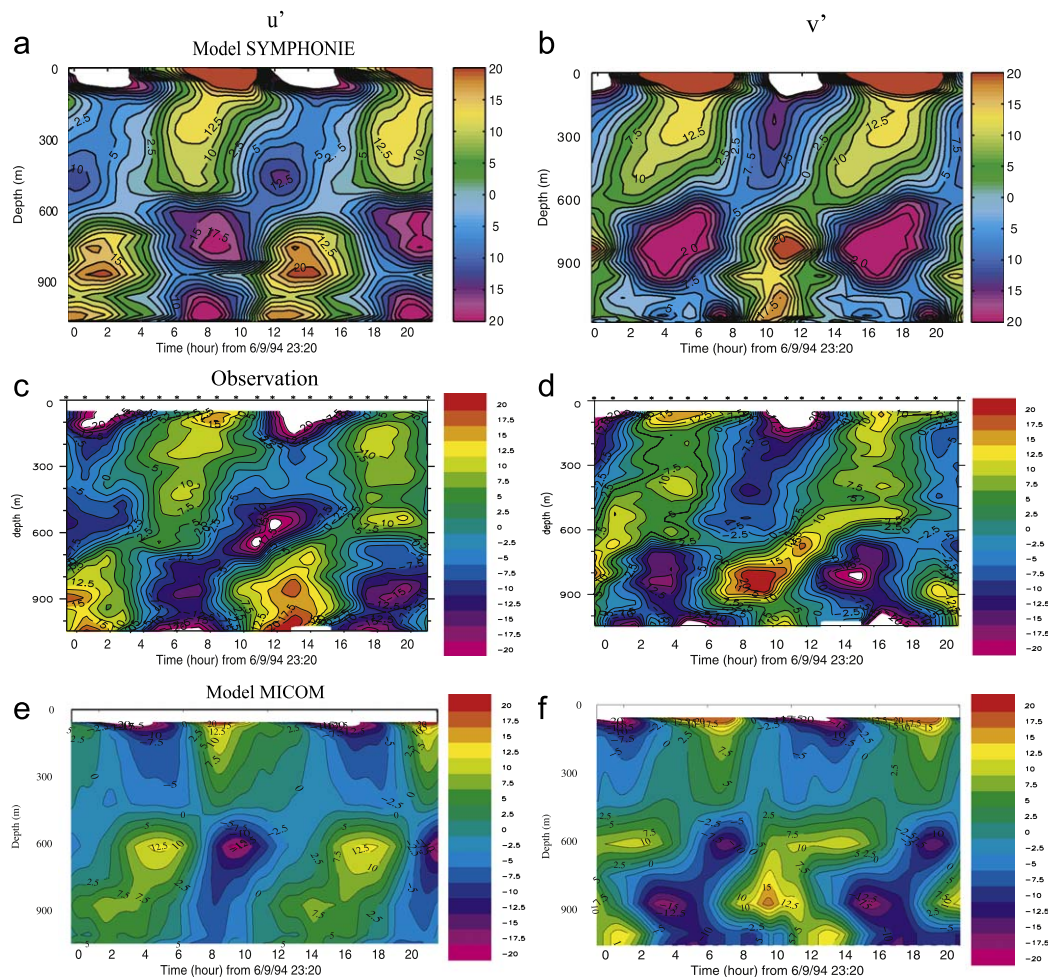

Fig. 6. Time series of baroclinic velocities $(cm\,s^{-1})$ at the PF6 location during two semi-diurnal tidal cycles (25 h): West–East component u' from the SYMPHONIE modeling (a), from lowered ADCP measurements (c) and from the MICOM modeling (e); South–North component v' from the SYMPHONIE modeling (b), from lowered ADCP measurements (d) and from the MICOM modeling (f). Courtesy of Scientia Marina, Figs. (c), (d), (e) and (f) are reproduced from Pichon and Correard (2006), respectively Figs. 16b, a, 15b and a.

3.4. Internal tide at the station PF6: comparison with observations

In this subsection, velocity profiles (Fig. 6) and density profiles (Fig. 7) from the model are compared with observations from the MINT94 experiment and with the solutions from the MICOM simulation at the station PF6 (on the radial S2, see Fig. 1).

The time evolution of the components of the baroclinic horizontal velocity (Fig. 6) looks nearly periodic, representing a semi-diurnal dominant propagation. There is a vertical shear of current between 500 and 700 m depth for the W–E component and near 600 m depth for the N–S component, due to a propagation dominated by the first mode as shown above. The maxima are located near the surface where the stratification is maximum and in the beam pathway (located between 600 and 900 m depth) where the current can reach values of more than $\pm 20\,\mathrm{cm\,s^{-1}}$. Another maximum is present close to the sea floor with a value of more than $17.5\,\mathrm{cm\,s^{-1}}$.

The time evolution of the isopycnal interfaces is plotted in Fig. 7. The semi-diurnal cycle is dominant again and the maximum amplitude occurs between depths of 500 and 900 m, with a maximum of 65 m centered around 850 m (Fig. 7 a). In the top layers, the vertical displacement is less than 30 m in the first 150 m (Fig. 7 b).

We show a comparison of these plots of velocity and density profiles with observations from Pichon and Correard (2006) (reproduced in Figs. 6 c, d and 7 c), showing a close agreement between the isopycnal and sigma models.

In particular, the vertical position of the current shears and the localization of the maxima of current in the vertical (even if they are sometimes weaker than the observed values) are well reproduced. The position of the maxima near the sea-bed in Fig. 6 b fits with the observations shown in Fig. 6 d. The secondary beams observed for instance at a depth of 900 m for both current components are well reproduced in the SYMPHONIE simulation. The accurate localization of the trajectory of the internal tide beam in the model may be enhanced by an accurate representation of local bathymetry gradients in the area of generation (use of generalized sigma coordinates in the vertical). In addition, the use of a large number of vertical levels allows for a fine representation of the width of the beam in the vertical. There is a phase difference of about 1–2 h between our simulation and the observation for both components of the current. Errors in the barotropic forcing (Pairaud et al., 2008) and the stratification may come into play.

Globally, the time series pattern for the density profile in Fig. 7 b resembles the one observed in the surface-layers (Fig. 7 c). This result can be considered as satisfactory since the initial density profile is uniform on the horizontal plane. But near the surface differences appear with a mixing tendency that makes the mean position of isopycnal surfaces evolve with time. For example the position of the $27\,\mathrm{kg\,m^{-3}}$ isopycnal surface has moved from a depth of 100 m to a depth of 115 m after 11 days (Fig. 7 b) due to mixing processes associated with the presence of internal tides and model mixing (through diffusion and advection schemes) in the absence of restratification mechanism. This vertical deepening
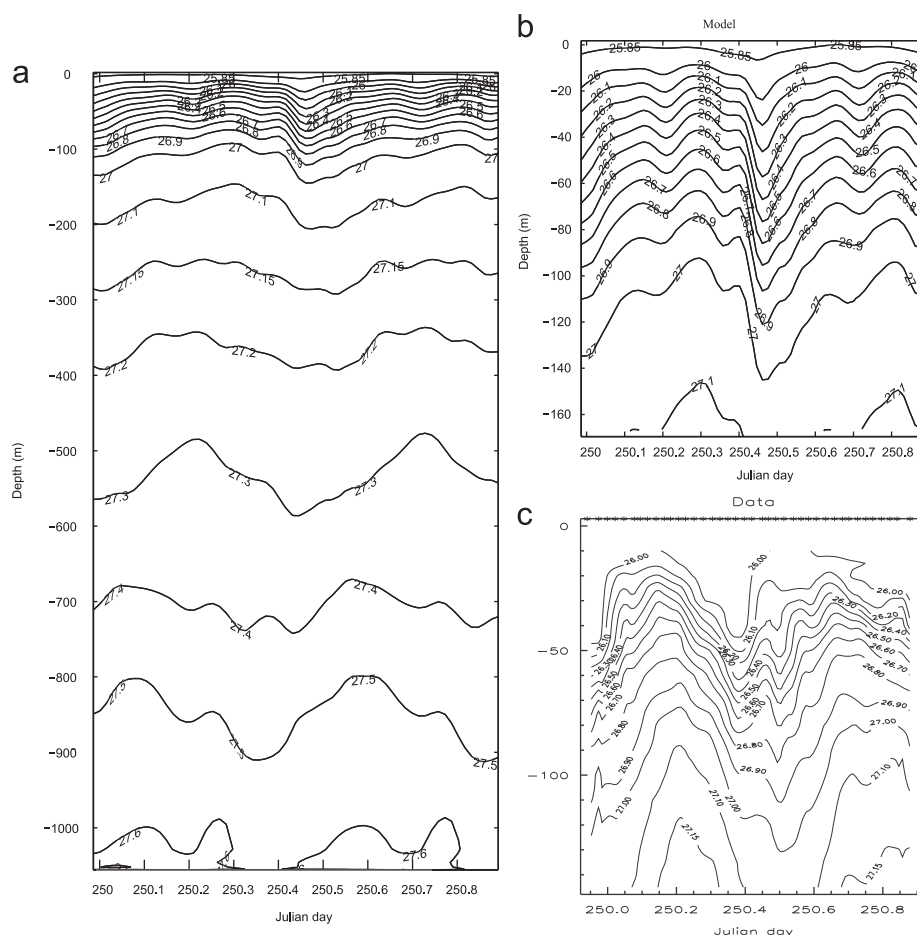

Fig. 7. Time evolution of isopycnal depths at the PF6 location during two semi-diurnal tidal cycles: (a) density profile given by the model, (b) same as (a) but for the first 170 m and (c) corresponding observed density profile from CTD stations for the first 150 m. Time is given in Julian days with 6/09 1994 (23:20 pm) as starting date. Courtesy of Scientia Marina, figure (c) is reproduced from Pichon and Correard (2006), Fig. 17b.

cannot be found in Fig. 7 c for the observed density profile. However, the station PF6 is located near one of the most important generation site for the internal tide in the Bay of Biscay and the mixing inducing a significant drift of isopycnics with time is restricted to this area. This was to be expected as no mechanism of restratification has been included.

The baroclinic currents modeled with SYMPHONIE (Figs. 6 a and b) have also been compared to those of MICOM (Figs. 6 e and f) (Pichon and Correard, 2006). The observed global pattern of the internal tide is well reproduced by both models (shears of current, positions of maxima of current, etc.). However, differences appear when comparing carefully the model results with observations. The phase lag from the observation for the E–W component of the current is only 1 h for the SYMPHONIE currents, against 2 h for the MICOM currents. Also, the maxima are more marked in the SYMPHONIE modeling, in good agreement with the observations, although they are too large near the surface. Maxima of bottom currents for the E–W component in the observation (Fig. 6 c) are well reproduced with the SYMPHONIE model (Fig. 6 a) but not with the MICOM model (Fig. 6 e). For the N–S component, Figs. 6 b, d and f show that the shear of current observed at about 600 m depth is well located in the SYMPHONIE modeling, whereas it is located near 500 m in the MICOM modeling. Thus, compared with observations (Figs. 6 c and d), the SYMPHONIE vertical current profiles are closer to the observations at the station PF6. The width of the beams is more accurately reproduced in our study as we use a higher number of vertical levels in the SYMPHONIE model (46) compared to the MICOM model (33). We use generalized sigma coordinates (instead of isopycnal coordinates in MICOM) and a slightly higher horizontal resolution (1.5 km instead of 1.8 km) which results in a better representation of the topography where the beams are generated and where they reflect. In addition, our barotropic tidal forcing includes a more complete tidal spectrum. Those differences have an impact over the good localization and amplitude of the beams.

The characteristics of internal tides owing to their frequency band will now be discussed.

4. WEof analysis of internal tides: generation of higher harmonics

4.1. Methodology

When studying internal tides, a common choice is to use harmonic analysis for extraction of the different components of the tidal spectrum. However, this techniques does not give any information about the tidal cycle. The combination of principal component analysis (PCA) and wavelet decomposition offers a promising alternative. This method called WEof analysis (for "Wavelet Empirical orthogonal functions") is described in details in Pairaud and Auclair (2005) as a combination of time-frequency wavelet analysis (Farge, 1992) and spatial PCA for the recognition of coherent physical structures. It consists of two steps, shortly described below.

First, in order to get the time and frequency localization of the waves, a one-dimensional continuous wavelet transform is applied on the time series of vertical velocity at each location using the complex Morlet wavelet (Torrence and Compo, 1988).

Then the second step consists of a principal component analysis (PCA) which allows a multivariate, multidimensional field to be decomposed into empirical orthogonal functions (Eofs). It provides an orthogonal basis whose vectors successively account for the maximum explained variance of the multivariate physical fields (Preisendorfer et al., 1981). In this study, a complex PCA is applied over a matrix of normalized wavelet coefficients, whose temporal mean has been removed, to give the dominant

singular vectors. PCA is performed through an "incomplete" singular value decomposition, i.e. only the k dominant singular values λ_i ($i = 1, 2, \ldots, k$) are considered. The variance explained by the i-th mode is defined by $\lambda_i / \sum_{j=1}^{k} \lambda_j$. This tool is of great interest because of the physical meaning of each of the basis vectors (Kutzbach, 1967). Many geophysical applications of the PCA intends to identify and study the physical meaning of the predominant modes of spatial variability across a given area.

The WEof analysis has been applied with success to the study and extraction of internal waves generated in idealized cases including several sources using the SYMPHONIE model, in a study by Pairaud and Auclair (2005). This study has shown that even though the Eofs are essentially statistical in nature and not necessarily physical, i.e. do not necessarily provide dynamical mode decomposition, in this specific case of internal gravity waves, they can be explained physically a posteriori. The WEof analysis was efficient in separating waves and in studying their transitory dynamics, and the use of Weofs led to refine our knowledge of the modal structure of the waves.

This method is used in the present paper to decorrelate internal tides with respect to their frequency band (semi-diurnal and quarter-diurnal) and to study their characteristics of generation and propagation. In particular the wavelengths and phase speeds of the internal tides are obtained in the same way as in the previous study by Pairaud and Auclair (2005). A focus on the reconstructed vertical velocity in a given frequency band leads to the recognition of the modal structure of internal tides and allows us to suggest generation and propagation schemes.

4.2. Generation and propagation of the semi-diurnal tide

A decomposition over the first six WEofs is completed for the semi-diurnal vertical velocity. The horizontal resolution for the analysis is coarser than for the numerical model. It is equal to 4.5 km (instead of 1.5 km) while 15 vertical levels are used (instead of 46). For the 3D PCA, 132 samples are considered with a time step of 1 h (for a total duration of 5.5 days). The analysis begins after 10.5 modeling days (on 6/09 at 12 am). The initial vertical velocity along the radial S′, the reconstructed semi-diurnal component and the first three WEofs are shown in Fig. 8 for 11/09 at 9 pm.

A wavelet analysis is first performed over the modeled vertical velocity field. The wave pattern of the semi-diurnal component along Section S′ (Fig. 8 b) is consistent with the global pattern (Fig. 8 a). This is due to the dominance of this component in the wave spectrum, M2 being the most energetic wave in the Bay of Biscay. With a pattern of propagation much less noisy than the original one, the maxima are less marked for the semi-diurnal reconstructed vertical velocity so that some energy spills over into other frequencies. The semi-diurnal internal tides are generated at the shelf break and then propagate over the abyssal plain from the Iberian slope and the Armorican slope (Fig. 8 b). Focusing on the waves propagating from the Armorican slope, the horizontal wavelength is $\lambda_H = 150 \pm 10$ km and fits with the theoretical value for Mode 1 ($\lambda_{H1,th} = 141$ km from Table 2). This result is similar to the wavelength found at a previous date when looking at the complete signal (Section 3). The dominance of a Mode 1 propagation in depth has also been noticed by Pichon and Correard (2006) in the case of a semi-diurnal imposed barotropic tidal forcing. In the top layer, the third mode dominates as for the multifrequency signal.

After the PCA of the semi-diurnal vertical velocity, WEofs are shown along the radial S′ in Figs. 8 c, e and f. There is a propagation from the Armorican slope that dominates along
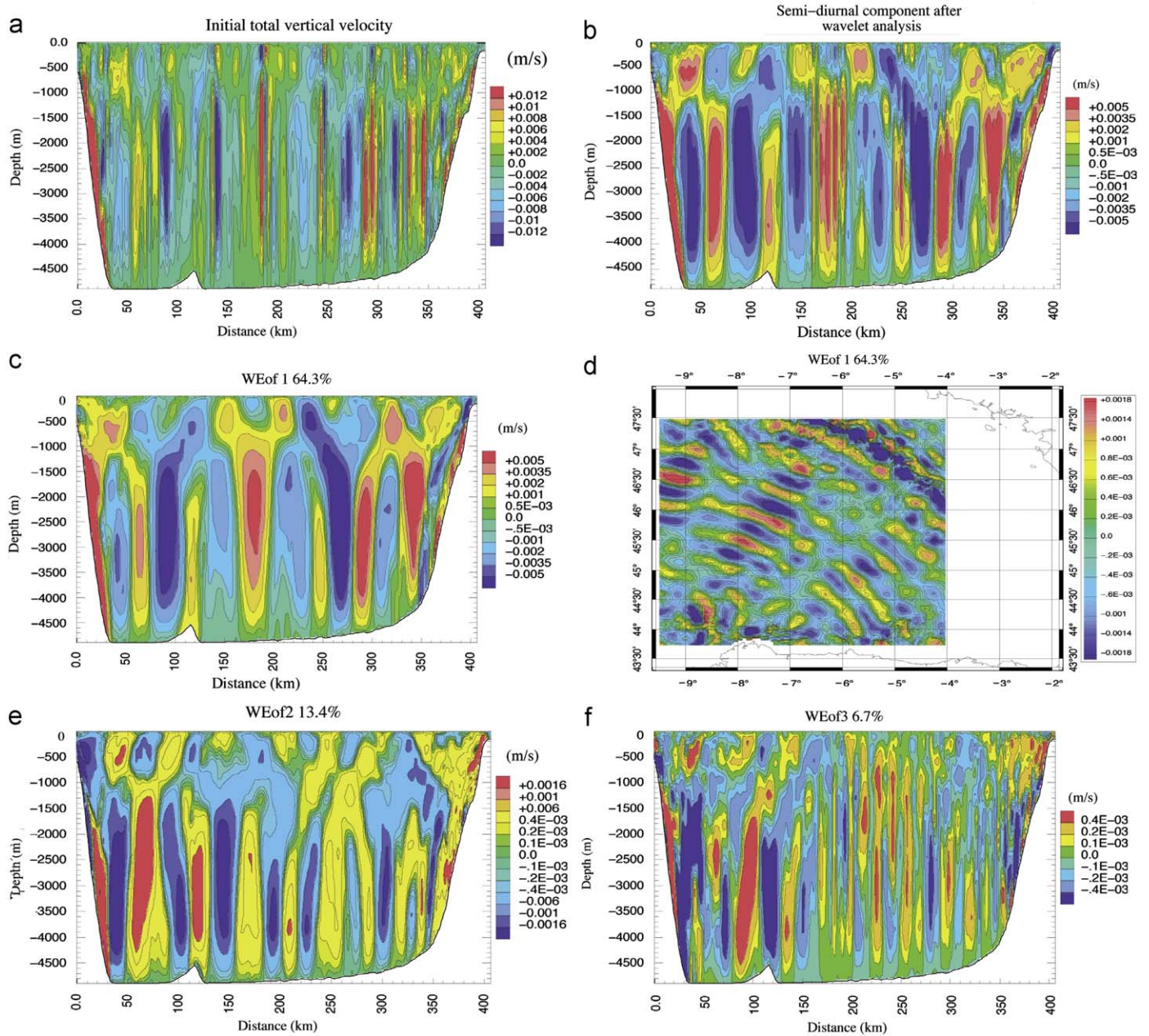
Fig. 8. WEof decomposition in the semi-diurnal frequency band for the Section S′ (with the french slope at the right of the plots): total vertical velocity, semi-diurnal vertical velocity and first three of six WEofs computed for the semi-diurnal vertical velocity (m s⁻¹) for 11/09 at 9:00 pm. (a) Total vertical velocity from the model, (b) reconstructed semi-diurnal vertical velocity using wavelet analysis, (c) WEof 1 accounting for 64.3% of the semi-diurnal vertical velocity variance with its horizontal pattern given by a section at 70 m depth on (d), (e) WEof 2 (13.4% of the field variance), (f) WEof 3 (6.7% of the field variance).

nearly all the radials, and a propagation from the Iberian slope that is dominant only over a few tens of kilometers.

The first WEof explains 64.3% of the semi-diurnal vertical velocity variance. It is shown in Fig. 8 c along the radial S′ and resembles the previous field of Fig. 8 b before the PCA. The dominant modal structure of the propagation is not modified, with an associated horizontal wavelength $\lambda_H = 149 \pm 7$ km, which is indicative for Mode 1. The time evolution of the WEof amplitude (not shown here) indicates that it is increasing rapidly in time until a few days after the spring tide, so that the amplitude follows the tidal cycle. A horizontal section at a depth of 70 m is shown in Fig. 8 d for the abyssal plain. This plot of the vertical velocity allows to confirm and refine the propagation pattern seen in Fig. 4 a. It contains only the semi-diurnal internal tide and shows a propagation dominated by Mode 3 in the surface layers over the abyssal plain, as noticed

previously for the total vertical velocity, with three major directions of propagation from the French slope. There is also a propagation from the Iberian side (approximately from (44.25N, 8.7W)), directed toward the East/North-East, that is better seen in Fig. 8 d than in Fig. 4 a for the total vertical velocity. It is associated with the propagation of the internal tide at the semi-diurnal frequency. This north-eastward propagation from an area close to the Ortegal Promontory off Spain has been identified in satellite imagery by Azevedo et al. (2006) and Da Silva et al. (2007). They evidenced the presence of "hotspots" off the northwest Iberian Peninsula, where strong internal tides crossing the thermocline produce internal solitary waves through non-linear effects. A comparison of our results with the SAR observations of Azevedo et al. (2006) shows that we reproduce similar patterns in the simulations. The direction of propagation of the internal tide from the Iberian side in Fig. 8 d for

WEof1 at the semi-diurnal frequency is close to the direction of propagation for the wave group of internal solitary waves observed by Azevedo et al. (2006, Fig. 6a, wave group 1). The multi-frequency map of vertical velocity (Fig. 4 a) exhibits a propagation pattern that may contain also another wave group observed by Azevedo et al. (2006, Fig. 7a, wave group 2), which results in a more northward propagation. A scheme of propagation including beams generated at different frequencies and including the non-linear processes remains to be found for this area. For this purpose, a non-hydrostatic simulation will be necessary to model the solitary waves.

The second WEof explains 13.4% of the field variance. The velocity maxima in Fig. 8 e are located near the generation areas with an extension from the Iberian shelf break. The modal structure of the internal tide changes along the radial. From the Iberian slope to 180 km offshore along S′, the horizontal wavelength is $\lambda_H = 52 \pm 3$ km, representative for a Mode 3 dominant propagation (with $\lambda_{H3,th} = 52$ km from Table 2). Between 180 and 240 km along the radial, the wavelength is much shorter, but this may be due to interferences of internal waves emanating from the two different slopes. Finally, the waves generated at the French slope propagate with a wavelength of about $\lambda_H = 65 \pm 10$ km, not far from the value for a pure Mode 2 propagation (with $\lambda_{H2,th} = 75$ km from Table 2).

The pattern of the propagation for WEof 3 looks like the pattern for WEof 2 in the South-Western part of the Section S′. This WEof explains 6.7% of the field variance. Between 30 and 140 km along the radial, the propagation is dominated by a mode close to Mode 3 with $\lambda_H = 47 \pm 3$ km from Fig. 8 f. In the second part of the radial, we are in the presence of higher modes.

With the help of the WEof analysis method, the propagation pattern of the internal tide at the semi-diurnal frequency is clarified. The presence of small scales is evidenced. Higher modes are propagating in addition to the dominant Mode 1 as highlighted in the deep layers. They reach their maximum domains of influence near the regions where the energy beams encounter the bottom, and their contribution to the internal tide rapidly decreases after a few tens of kilometers. Further dedicated studies may specify the exact generation mechanism of these modes.

4.3. Generation of higher harmonics

In the Bay of Biscay, interactions of the reflected beams can induce non-linear effects. In what follows, we investigate the generation of the quarter-diurnal internal tide (M4) together with its propagation after a WEof analysis (as was done for the semi-diurnal components). An important point is how the generation of the M4 internal tide occurs during the propagation of the semi-diurnal component in a realistic case with varying stratification and slopes.

A linear internal tide forcing can induce a non-linear response involving higher harmonics (waves whose frequencies are for example double of that of the primary waves) when the beams reflect at a surface or via self-advection. This process is likely to happen in the overlapping region of the incoming and reflected beams at the ocean floor or near the surface, but also in areas where the stratification is strongly varying (like in a thermocline). Several theoretical, numerical and experimental studies have been carried out in order to understand the generation of higher harmonics when the wave beams reflect from a sloping bottom in the case of a uniformly stratified fluid. Tabaei et al. (2005) and Gerkema (2006) give a theoretical description of the generation of higher harmonics from the reflection of a monochromatic internal wave in the non-hydrostatic case (without and with rotation). A numerical study from Gerkema et al. (2006) has shown that in the case of a continuously stratified rotating fluid while assuming

uniformity in the along-slope direction, higher harmonics were generated at the bottom of the ocean where the M2 beam was reflecting. Recent laboratory experiments by Peacock and Tabaei (2005) have illustrated the generation of second harmonics at a sloping bottom and Gostiaux et al. (2006) have dealt with the second and third harmonics.

According to the linear theory, the propagation of the internal tide at M4 frequency requires that $\omega_{M4} = 2\omega_{M2} < N$. This is the case for the M4 wave in the MINT94 experiment if a mean value is taken for N ($\omega_{M4} = 2.8 \times 10^{-4}$ rad s^{-1} and $N = 1.5 \times 10^{-3}$ s^{-1}).

In Figs. 9 a and b, vertical velocities are shown along the radial S after a wavelet analysis at both semi-diurnal and quarter-diurnal frequencies. The semi-diurnal component (Fig. 9a, after 14 days) is maximum close to the generation area, and the vertical velocity tends to decrease after the beam has crossed a short distance, even after the first reflection of the beam. Actually, the value decreases from more than 0.7×10^{-2} m s^{-1} before the first reflection to half this value near 200 km along the radial.

The map of the quarter-diurnal internal tide in Fig. 9 b shows beams that are steeper than those at the semi-diurnal frequency, owing to their frequency which modifies the slope of the beam (see Eq. (1)). The vertical velocity for the M4 internal tide reaches a maximum of 0.4×10^{-2} m s^{-1}, which is approximately half the value for the semi-diurnal component. Two regions of maximum vertical velocity are shown, localized between 130 and 220 km and between 265 and 300 km along the radial S (Fig. 9 b). This supports the idea of several generation areas for the M4 internal tide. First, internal waves at M4 frequency are generated at the shelf break due to a forcing by the M4 barotropic tide. But they are not very energetic and vanish faster than the semi-diurnal internal tides. Then, a second generation of the M4 internal tide occurs over the abyssal plain during the propagation of semi-diurnal internal tides in the middle of the Bay of Biscay. The non-linear interaction of the incoming and outgoing beams in the region of the reflection of M2 gives birth to an internal tide at M4 frequency, as the non-linear terms become non-zero in the equations (Tabaei et al., 2005). This process was also illustrated in the study by Grisouard et al. (2008, Fig. 8). A careful inspection of the propagation on plots of the velocity phase (not shown here) shows that the generation of a M4 internal tide happens in the upper water column. We thus suggest that the thermocline under the surface mixed layer is a possible additional place for the generation of the M4 internal tide.

Two origins were thus found for the generation of the M4 internal tide, one being the well-known barotropic forcing at M4 frequency over the slope, and the other being a forcing by non-linear interactions of the internal component at the semi-diurnal frequency in the middle of the Bay of Biscay, in the first hundred meters along the water column, where the incident tidal beam is reflected from the near-surface.

The reconstructed WEof pattern for the vertical velocity along the radial S′ at the quarter-diurnal frequency (not shown here) is similar to the one found for the semi-diurnal component. Higher modes are visible in the deep ocean as for the semi-diurnal tide. In addition, the semi-diurnal WEof 3 is dominated by the third mode in the first half of the radial (that is waves propagating with a wavelength close to 50 km in Fig. 8). From Table 2, the wavelength for M4 Mode 1 internal waves is of the order of 49 km. This is approximately the value found for both the semi-diurnal WEof 3 and the quarter-diurnal WEof 1 at the same place. Therefore the generation of M4 internal tide may be favored by this wavelength adequacy.

A map of the vertical displacement induced by the propagation of the M4 internal tide along the radial S2 is shown in Fig. 10. The maxima reach more than 30 m, i.e. nearly half the maximum value for the semi-diurnal component over the abyssal plain (see Fig. 5 b for the same picture at the semi-diurnal frequency). Locally, the quarter-diurnal contribution cannot be neglected
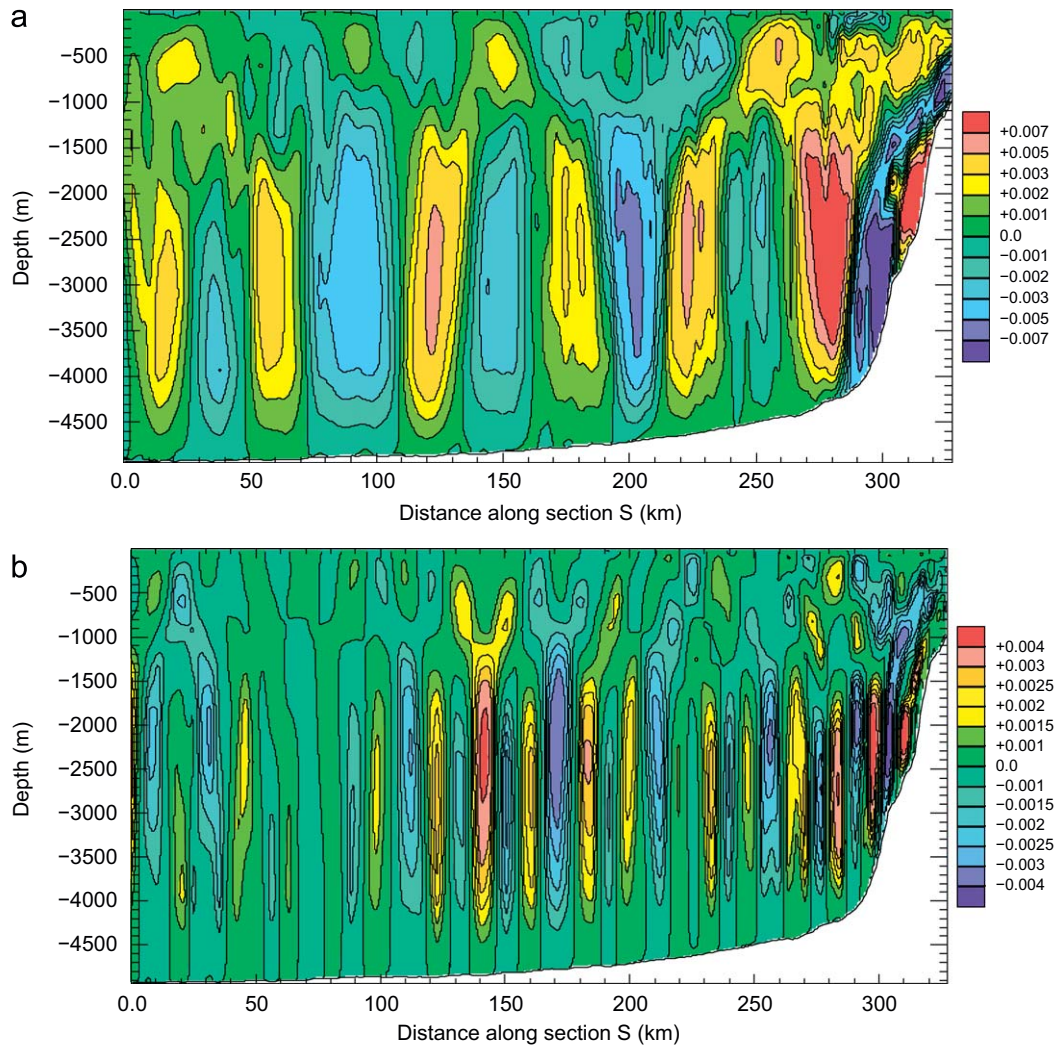
a

b

Fig. 9. Reconstructed vertical velocities (m s^{-1}) along the Section S for 9/09 at 7:00 pm with a horizontal resolution of 4.5 km over 15 vertical levels: (a) for the semi-diurnal component of the spectrum and (b) for the quarter-diurnal component.
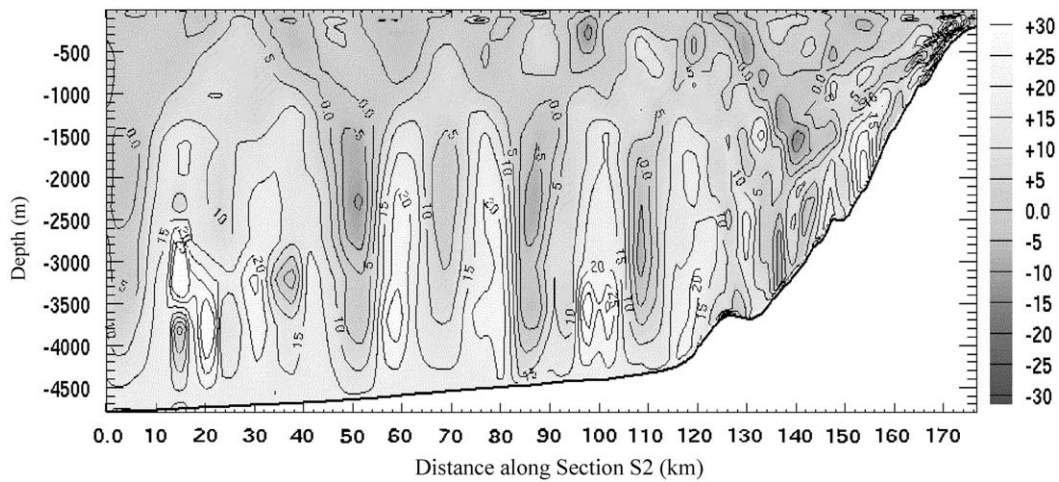

Fig. 10. Vertical displacement (m) of isopycnal surfaces for the quarter-diurnal component of the internal tide along S2 for 9/09 at 9:00 pm. (a) Horizontal of vertical velocity at 70 m depth for 10/08 2003 at 12:00 am (m s^{-1}) after 9.5 days. Along the white radial, called Sp [(44.3N,9.4W),(47.7N,6.9W)], (b) shows the salinity (psu) on the vertical with the presence of salted Mediterranean water near the Iberian slope and (c) shows the total longitudinal horizontal velocity along the radial over the abyssal plain with bold dashed lines representing the paths of the characteristic rays. In frames b and c, F and I corresponds to the French and Iberian side of the section, respectively.

when studying the mixing processes attributed to the internal tide. As a consequence, M4 barotropic component must be taken into account for the study of the internal tide in the Bay of Biscay and the forcing at the boundary by M4 barotropic tidal currents must be included because it has an impact over the slope currents.

5. Sensitivity to initial stratification using a three-dimensional POP summer stratification

Although the internal tides have been validated and explored independently owing to their frequency, the impact of making assumptions on the stratification remains unknown. Using an initial one-dimensional stratification instead of a fully three-dimensional stratification facilitates the understanding of how internal tide propagates in the model. In this section, an embedding strategy is implemented in the Bay of Biscay (Auclair et al., 2006).

The model of the Bay of Biscay is initialized and forced with the three-dimensional fields of horizontal velocities, sea surface elevation, temperature and salinity of a POP monthly climatology for the month of August (B. Levier, pers. comm.). These fields were obtained by averaging the POP 1/10 degree model outputs over 5 years (Friocourt et al., 2007). As both the bathymetry and the physics of each model differ, the physical field used to force the small scale model has to be dynamically adjusted. The main issue is to reduce the spin-up while incorporating the information provided by the larger scale model. This is achieved using the VIFOP variational initialization tool (Auclair et al., 2000a, 2006). The interpolation of the large scale physical fields over the smaller grid is performed so that the variational constraints associated with the larger scale oceanic model dynamics are minimized and the fundamental mass budgets are respected.

Fig. 11a shows a horizontal section of the vertical velocity at 70 m depth in the seasonal thermocline. The main direction of
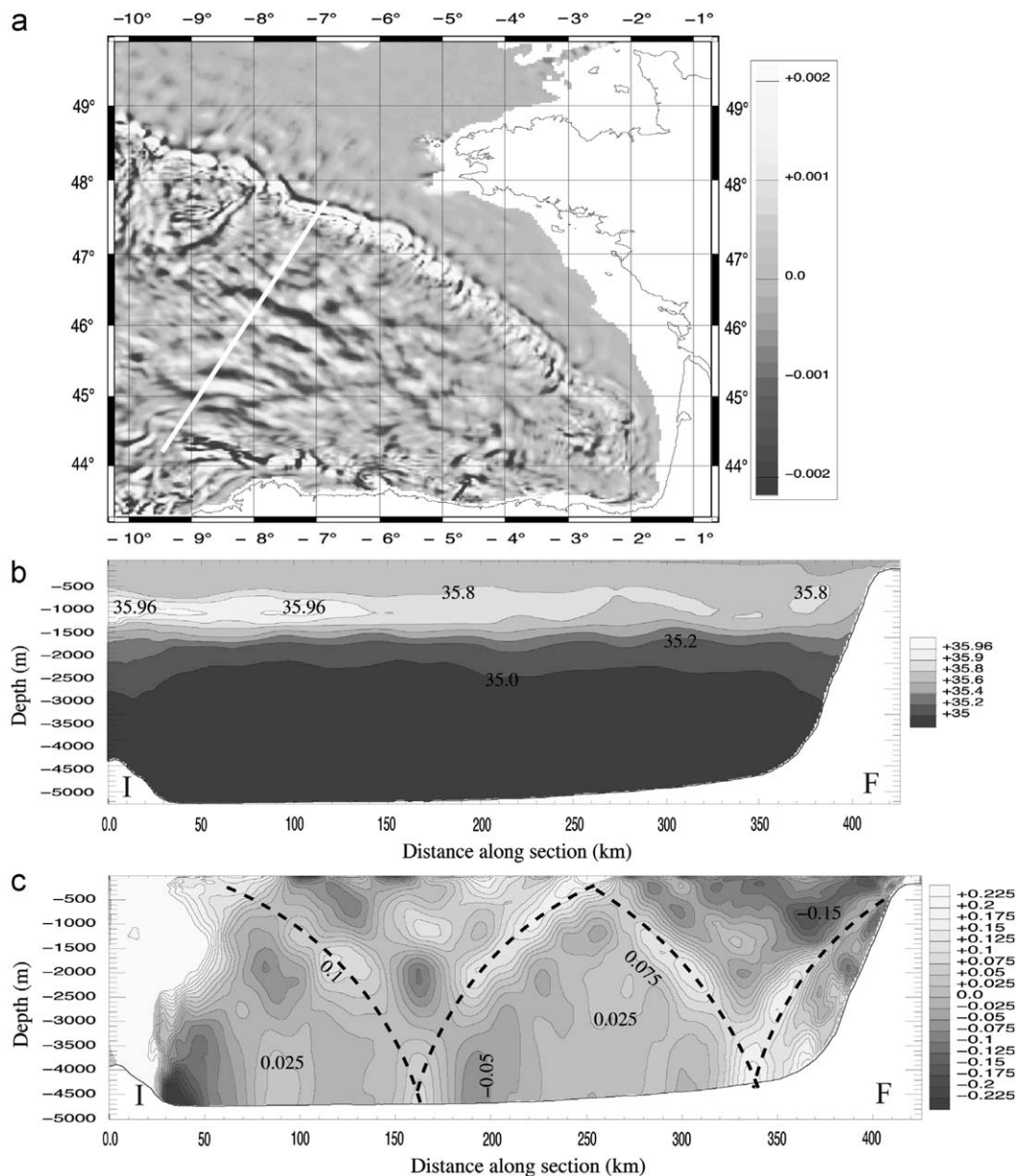

Fig. 11. (a) Horizontal section of vertical velocity at 70 m depth for 10/08 2003 at 12:00 am (m s^{-1}) after 9.5 days. Along the white radial, called Sp [(44.3N,9.4W),(47.7N,6.9W)], (b) shows the salinity (psu) on the vertical with the presence of salted Mediterranean water near the Iberian slope and (c) shows the total longitudinal horizontal velocity along the radial over the abyssal plain with bold dashed lines representing the paths of the characteristic rays. In frames b and c, F and I correspond to the French and Iberian side of the section, respectively.

propagation of the internal tide from La Chapelle bank is somehow different from what was found in the MINT94 experiment (see Fig. 4 a as a comparison). In the following, we thus choose to show vertical sections along the radial Sp (white line in Fig. 11 a) for the POP experiment.

Fig. 11 b shows the initial salinity over the plain along the radial Sp. It is an illustration of the horizontal non-homogeneity of the stratification. Hot and salty Mediterranean water enters the domain by its southern part, then flows northwards above the slope. The signature of this water mass is recognizable on the plot with salinities reaching nearly 36 psu along the radial Sp on the Iberian side. The depth of the core of the Mediterranean water mass is at about 900 m, so that it is correctly located in the forcing field. This maximum of salinity and heat contributes to the horizontal non-homogeneity of the stratification.

As in Fig. 4 a, Fig. 11 a shows internal waves propagating from the slope towards the abyssal plain as well as toward the coast. As for the MINT94 modeling, the most energetic propagation appears above the plain with higher vertical velocities. However, several differences are visible from a comparison with Fig. 4 a. Firstly, favored directions of propagation are less obvious. There is only one favored radial above the abyssal plain that dominates, around the radial Sp. In the case of the three-dimensional stratification, the internal tides propagating from the Iberian side look stronger, with higher values of the associated vertical velocity. The propagation from the Iberian slope is directed more northward compared with the MINT94 case. Over the shelf, vertical velocities are weaker and the internal tide is not seen to propagate far over. The stratification, associated with the presence of wind forcing, river plumes or tidal fronts (off Ouessant) for instance, may prevent the tide from propagating further into the shelf.

For the vertical structure of the internal tide, the plot of the longitudinal horizontal velocity along Section Sp in Fig. 11 c shows that the beams penetrate deeper inside the water column compared to what was found for the MINT94 experiment (see Fig. 4 b for example). The reflection of the main beam at the bottom occurs at 65 ± 10 km from the upper slope, against approximately 45 km in the case of waves propagating along the MINT94 S2 radial (Fig. 5). The horizontal wavelength is of the order of 190 ± 10 km, against approximately 150 km in the case of waves propagating along the MINT94 S' radial (Fig. 4 b). Horizontal and vertical scales of the internal tides are therefore different in the two cases. At the left end of the radial, on the Iberian side, large horizontal velocities are visible from the figure.

From this experiment, the initial stratification is found to be a source of large inhomogeneities in the internal tide pattern in the Bay of Biscay. The use of an initial three-dimensional stratification including the Mediterranean water and the signature of other processes, plus the forcing by the general circulation, is likely to modify the direction of propagation of the waves emanating from the Iberian slope. The large generation at the Iberian slope could be associated with the generation over the seamount at this location and by the interactions between the different waves propagating in this area. Over the shelf, the complex combination of processes results in a rapid damping of the internal tide.

6. Conclusion

Barotropic tides in the Bay of Biscay have a very large amplitude. A large amount of barotropic energy is dissipated over the continental shelf, especially at the entrance of the English Channel (Pairaud et al., 2008). In addition to bottom friction effects, a part of this energy is dissipated via the generation of the internal tides. When crossing the shelf break, barotropic currents

are nearly perpendicular to bathymetry gradients and internal tides are generated over the topography.

In this study, the SYMPHONIE model was applied to the modeling of the MINT94 experiment. We obtained a good agreement with the observations for both barotropic and baroclinic tides. In particular, the position of energy maxima for the internal tide (beams) and the amplitude of the oscillations were well reproduced. The process of generation of the internal tide is very sensitive to the bottom slope. Generation areas were found to be over the shelf break and slope, as was previously observed for example by Pingree and New (1991). Comparing the characteristics of internal tides found in this study with in situ and satellite images from the literature, we have validated and confirmed some aspects of the propagation. One example is the existence of several generation area in the southern Bay of Biscay from which the internal tides propagate (Da Silva et al., 2007).

An original comparison of σ and isopycnal modeling has been carried out. It has been shown that reasonable agreement could be achieved between the two approaches, the inviscid nature of the latter providing an interesting basis of comparison for the former. An extension of the isopycnal modeling to the shelf (and the mixing layer) has also been proposed.

A space–time WEof analysis of the internal tide in the Bay of Biscay has shown that for semi-diurnal and quarter-diurnal components, higher modes were visible locally in the deep ocean in addition to the dominant Mode 1. The spectrum content of internal tides in the Bay of Biscay includes a non-negligible quarter-diurnal supply. A part of the M4 internal tide was found to be due to the interaction of M4 barotropic tide with the topography. As in the case of a pure M2 internal tide reflecting at the surface in an ocean of constant stratification N (Grisouard et al., 2008), the M4 internal tide was also generated through non-linearities at the reflection of the M2 internal tide in the middle of the Bay of Biscay under the surface mixed layer. The vertical displacement associated with the M4 internal tide can be up to half that of the semi-diurnal component in some areas, with a significant impact on the stratification of the ocean. The internal tide at the M4 frequency has thus to be fully considered in future studies dealing with the computation of energy budgets and with the quantification of mixing.

Whereas analytical studies often restrict themselves to a two-dimensional ocean forced by a monochromatic wave in a two or three layer water column (e.g. Baines, 1982), it is important to take into account the three-dimensionality of the problem to deal with internal tides. In this study, we needed to consider the real stratification of the Bay of Biscay and we needed to restrict ourselves to simplified studies. After using a one-dimensional vertical density profile, we thus investigated the consequences of using a three-dimensional initial stratification. A POP monthly stratification (B. Levier, pers. comm.) was used for this purpose. Significant differences from the MINT94 experiment appeared in the generation and propagation of the internal tide. The major directions of propagation over the plain were modified (more N–S oriented in the POP experiment) and the intensity of the internal tide was changed. The stratification and the presence of barotropic currents play a role over the shelf and prevent the internal tide from propagating far onto the shelf in the POP experiment, whereas its signature was seen close to the coast in the MINT94 experiment.

From this study, our knowledge of the dynamics of internal tides in the Bay of Biscay has been enhanced, but the role of internal tides in mixing for a realistic (stratification and bathymetry) case and the associated energy transfers remain to be quantified.

Acknowledgments

Appendix A. Computation of the vertical displacement of isopycnal surfaces

Vertical motions induce a change in the position of isopycnal surfaces at the tidal frequency.

The vertical displacement is computed relatively to the mean position for each tidal cycle. In the present case the use of a sigma coordinate model makes difficult the computation of the internal tide amplitude because it is necessary to invert $\rho(z)$ to obtain $z(\rho)$.

Gill (1982) and Nash et al. (2005) suggest that the vertical displacement of an isopycnal surface $\xi(z,t)$ relative to its mean position is linked to the density anomaly $\rho'(z,t)=\rho(z,t)\text{-}\overline{\rho}(z)$ where $\rho(z,t)$ is the instantaneous measured density and $\overline{\rho}(z)$ is the time mean vertical density profile. The relationship is then given by $\xi(z,t)=(g/\overline{\rho})(1/\overline{N^2})\rho'(z,t)$ and uses a mean Brunt–Väisälä frequency. A difficulty in using this computation appears in the present study since $\overline{N}$ has a meaning only if computed locally because of rapid variations of N with depth when crossing the thermocline.

A direct method is therefore preferred in order to compute $\rho(z)$ from $z(\rho)$. The following algorithm is used:

- get the depth of isopycnal surfaces at time $t=0$ at each sigma level,
- follow step by step the depth of isopycnal surfaces: at each location and at each time step (or at a short enough time interval, of order a few minutes in the framework of this study) the algorithm interpolates the depth of the isopycnal surfaces with regard to their previous position on the vertical.

At last, for the study needs, the forcing is multifrequency. In order to consider only the displacement of isopycnal surfaces due to the propagation of internal waves and to distinguish the effects of the different tidal components, the displacements of vertical isopycnal surfaces $z(\rho)$ are analyzed by the wavelet method.

References

Arakawa, A., Lamb, V.R., 1977. Computational design of the basic dynamical processes of the UCLA general circulation model. Meth. Comput. Phys. 17, 174–267.

Auclair, F., Casitas, S., Marsaleix, P., 2000a. Application of an inverse method to coastal modelling. J. Atmos. Ocean. Technol. 17, 1368–1391.

Auclair, F., Marsaleix, P., Estournel, C., 2000b. Sigma coordinate pressure gradient errors: evaluation and reduction by an inverse method. J. Atmos. Ocean. Technol. 17, 1348–1367.

Auclair, F., Estournel, C., Marsaleix, P., Pairaud, I., 2006. On coastal ocean embedded modeling. Geophys. Res. Lett. 33, L14602, doi: 10.1029/2006GL026099.

Azevedo, A., da Silva, J.C.B., New, A.L., 2006. On the generation and propagation of internal solitary waves in the southern bay of Biscay. Deep-Sea Res. 53 (6), 927–941, doi: 10.1016/j.dsr.2006.01.013.

Baines, P.G., 1973. The generation of internal tides by flat-bump topography. Deep-Sea Res. 20, 179–205.

Baines, P.G., 1974. The generation of internal tides over steep continental slopes. Philos. Trans. R. Soc. London 277A, 27–58.

Baines, P.G., 1982. On internal tide generation models. Deep-Sea Res. 29, 307–338.

Beckmann, A., Haidvogel, D.B., 1993. Numerical simulation of flow around a tall isolated seamount. Part i: Problem formulation and model accuracy. J. Phys. Oceanogr. 23, 1736–1753.

Bell, T.H., 1975. Topographically generated internal waves in the open ocean. J. Geophys. Res. 80 (3), 320–338.

Blumberg, A.F., Mellor, G., 1987. A description of a three dimensional coastal circulation model. Three dimensional coastal ocean model. N. Heaps, AGU, Washington, DC, 208pp.

Cacchione, D.A., Drake, D.E., 1986. Nepheloid layers and internal waves over continental shelves and slopes. Geo-Mar. Lett. 6, 147–152.

Cox, C.S., Sandstrom, H., 1962. Coupling of internal and surface waves in water of variable depth. J. Oceanogr. Soc. Japan 30th Anniversary, 449–513.

Craig, P.D., 1987. Solutions for internal tide generation over coastal topography. J. Mar. Res. 45, 83–105.

Cummins, P.F., Oey, L.Y., 1997. Simulation of barotropic and baroclinic tides off northern British Columbia. J. Phys. Oceanogr. 27, 762–781.

Da Silva, J.C.B., New, A.L., Azevedo, A., 2007. On the role of SAR for observing local generation of internal solitary waves off the Iberian Peninsula. Can. J. Remote Sensing 33 (5), 388–403.

Egbert, G.D., Ray, R.D., 2001. Estimates of M2 tidal energy dissipation from topex/poseidon altimeter data. J. Geophys. Res. 106 22,475–22,502.

Farge, M., 1992. Wavelet transforms and their application to turbulence. Annu. Rev. Fluid Mech. 24, 395–457.

Flather, R.A., 1976. A tidal model of the northwest European continental shelf. Mem. Soc. R. Sci. Liège 10, 141–164.

Friocourt, Y., Levier, B., Speich, S., Blanke, B., Drijhout, S.S., 2007. A regional numerical ocean model of the circulation in the Bay of Biscay. J. Geophys. Res. 112 (C9 doi:10.1029/2006JC003935.

Garrett, C., Kunze, E., 2007. Internal tide generation in the deep ocean. Annu. Rev. Fluid Mech. 39 (1), 57–87.

Garrett, C., St Laurent, L., 2002. Aspects of deep ocean mixing. J. Oceanogr. 58, 11–24.

Gaspar, P., Gregoris, Y., Lefevre, J.M., 1990. A simple eddy-kinetic-energy model for simulations of the oceanic vertical mixing: tests at station Papa and long-term upper ocean study site. J. Geophys. Res. 95 16,179–16,193.

Gerkema, T., 2006. Internal-wave reflection from uniform slopes: higher harmonics and Coriolis effects. Nonl. Proc. Geophys. 13, 265–273.

Gerkema, T., Lam, F.P.A., Maas, L.R.M., 2004. Internal tides in the Bay of Biscay: conversion rates and seasonal effects. Deep-Sea Res. 51, 2995–3008.

Gerkema, T., Staquet, C., Bouruet-Aubertot, P., 2006. Non-linear effects in internal-tide beams, and mixing. Ocean Model. 12, 302–318.

Gill, A.E., 1982. Atmosphere-Ocean Dynamics. Academic Press, New York 662pp.

Gostiaux, L., Dauxois, T., 2007. Laboratory experiments on the generation of internal tidal beams over steep slopes. Phys. Fluids 19 (1), 1–4.

Gostiaux, L., Dauxois, T., Didelle, H., Sommeria, J., Viboud, S., 2006. Quantitative laboratory observations of internal wave reflexion on ascending slopes. Phys. Fluids 18 doi:10.1063/1.2197528, 056602.

Grisouard, N., Staquet, C., Pairaud, I., 2008. Numerical simulation of a two-dimensional internal wave attractor. J. Fluid Mech. 614, 1–14.

Hibiya, T., 2004. Internal wave generation by tidal flow over a continental slope. J. Oceanogr. 60 (3), 637–643, doi: 10.1023/B:JOCE.000003856.45342.6c.

Holloway, P.E., 1996. A numerical model of internal tides with application to the Australian north west shelf. J. Phys. Oceanogr. 26, 21–37.

Jezequel, N., Maze, R., Pichon, A., 2002. Interaction of a semidiurnal tide with a continental slope in a continuously stratified ocean. Deep-Sea Res. 49, 707–734.

Khatiwala, S., 2003. Generation of internal tides in an ocean of finite depth: analytical and numerical calculations. Deep-Sea Res. 50, 3–21.

Kutzbach, J.E., 1967. Empirical eigenvectors of sea-level pressure, surface temperature and precipitation complexes over North America. J. Appl. Meteorol. 6, 791–802.

Legg, S., 2004. Internal tides generated on a corrugated continental slope. Part i: cross-slope barotropic forcing. J. Phys. Oceanogr. 34 (1), 156–173.

Llewellyn Smith, S.G., Young, W.R., 2002. Conversion of the barotropic tide. J. Phys. Oceanogr. 32, 1554–1566.

Lyard, F., Le Provost, C., 1997. Energy budget of the tidal hydrodynamic model FES94.1. Geophys. Res. Lett. 24, 687–690.

Marsaleix, P., Auclair, F., Estournel, C., 2006. Considerations on open boundary conditions for regional and coastal ocean models. J. Atmos. Ocean. Technol. 23 (11), 1604–1613, doi: 10.1175/JTECH1930.1.

Marsaleix, P., Auclair, F., Floor, J.W., Herrmann, M.J., Estournel, C., Pairaud, I., Ulses, C., 2008. Energy conservation issues in sigma-coordinate free-surface ocean models. Ocean Model. 20, 61–89, doi: 10.1016/j.ocemod.2007.07.005.

Merrifield, M.A., Holloway, P.E., 2002. Model estimates of M2 internal tide energetics at the Hawaiian ridge. J. Geophys. Res. 107 (C8), 3179, doi: 10.1029/2001JC00996.

Mowbray, D.E., Rarity, B.S., 1967. A theoretical and experimental investigation of the phase configuration of internal waves of small amplitude in a density stratified liquid. J. Fluid Mech. 28, 1–16.

Munk, W., Wunsch, C., 1998. Abyssal recipes ii: energetics of tidal and wind mixing. Deep-Sea Res. 45, 1976–2000.

Munroe, J.R., Lamb, K.G., 2005. Topographic amplitude dependence of internal wave generation by tidal forcing over idealized three-dimensional topography. J. Geophys. Res. 110, C02001, doi: 10.1029/2004JC002537.

Nash, J.D., Alford, M.H., Kunze, E., 2005. Estimating internal wave energy fluxes in the ocean. J. Atmos. Ocean. Technol. 22, 1551–1570.

New, A.L., 1988. Internal tidal mixing in the bay of Biscay. Deep-Sea Res. 35 (5), 691–709.

New, A.L., Da Silva, J.C.B., 2002. Remote-sensing evidence for the local generation of internal soliton packets in the central Bay of Biscay. Deep Sea Res. 49, 915–934.

New, A.L., Pingree, R.D., 1990. Large-amplitude internal soliton packets in the central Bay of Biscay. Deep Sea Res. 37, 513–524.

Niwa, Y., Toshiyuki, H., 2004. Three-dimensional numerical simulation of the M2 internal tides in the east China sea. J. Geophys. Res. 109 doi:10.1029/2004JC001923.

Pairaud, I., Auclair, F., 2005. Combined wavelet and principal component analysis (WEof) of a scale-oriented model of coastal ocean gravity waves. Dynam. Atmos. Oceans 40 (4), 254–282.

Pairaud, I.L., Lyard, F., Auclair, F., Letellier, T., Marsaleix, P., 2008. Dynamics of the semi-diurnal and quarter-diurnal internal tides in the Bay of Biscay. Part 1: barotropic tides. Cont. Shelf Res. 28 (10–11), 1294–1315, doi: 10.1016/j.csr.2008.03.004.

Peacock, T., Tabaei, A., 2005. Vizualisation of nonlinear effects in reflecting internal waves beams. Phys. Fluids 17, 1–4.

Pichon, A., Correard, S., 2006. Internal tides modelling in the bay of Biscay. Comparisons with observations. Sci. Mar. 70S1, 68–88.

Pingree, R.D., Mardell, G.T., 1981. Slope turbulence, internal waves and phytoplankton growth at the Celtic Sea shelf break. Philos. Trans. R. Soc. London 302, 663–682.

Pingree, R.D., New, A.L., 1989. Downward propagation of internal tidal energy into the Bay of Biscay. Deep-Sea Res. 36, 735–758.

Pingree, R.D., New, A.L., 1991. Abyssal penetration and bottom reflection of internal tidal energy in the Bay of Biscay. J. Phys. Oceanogr. 21, 28–39.

Pingree, R.D., New, A.L., 1995. Structure, seasonal development and sunglint spatial coherence of the internal tide on the Celtic and Armorican shelves and in the bay of Biscay. Deep-Sea Res. 42, 245–284.

Pingree, R.D., Mardell, G.T., New, A.L., 1986. Propagation of internal tides from the upper slopes of the bay of Biscay. Nature 321, 154–158.

Pinkle, R., Rudnick, D., 2006. Tidal conversion and ocean mixing processes at Kanea ridge Hawaii. J. Phys. Oceanogr. 36, 965–966.

Preisendorfer, R., Zwiers, F., Barnett, T., 1981. Foundations of principal component selection rules. Scripps Institute of Oceanography Report, pp. 81–87.

Prinsenberg, S.J., Rattray, M., 1975. Effects of continental slope and variable Brunt–Vaisala frequency on the coastal generation of internal tides. Deep-Sea Res. 22, 251–263.

Rattray, M., 1960. On the coastal generation of internal tides. Tellus 12, 54–62.

Robertson, R., 2001. Internal tides in the southern Weddell Sea 1. Model description. J. Geophys. Res. 106 (C11), 27,001–27,016.

Saenko, O.A., 2006. The effect of localized mixing on the ocean circulation and time-dependent climate change. J. Phys. Oceanogr. 36, 140–160.

Simmons, H.L., Jayne, S.R., St Laurent, L.C., Weaver, A.J., 2004. Tidally driven mixing in a numerical model of the ocean general circulation. Ocean Model. 405, 775–778.

St Laurent, L.C., Garrett, C., 2002. The role of internal tides in mixing the deep ocean. J. Phys. Oceanogr. 32, 2882–2899.

Tabaei, A., Akylas, T.R., Lamb, K.G., 2005. Nonlinear effects in reflecting and colliding internal wave beams. J. Fluid Mech. 526, 217–243.

Torrence, C., Compo, G.P., 1988. A practical guide to wavelet analysis. Bull. Am. Meteorol. Soc. 79, 61–78.

Ulses, C., Estournel, C., Bonnin, J., Durrieu de Madron, X., Marsaleix, P., 2008. Impact of storms and dense water cascading on shelf-slope exchanges in the gulf of Lion (NW Mediterranean). J. Geophys. Res. 113 (C02010), doi:10.1029/2006JC003795.

van Aken, H.M., 2000. The hydrography of the mid-latitude northeast Atlantic ocean. ii: The intermediate water masses. Deep-Sea Res. 47, 789–824.

Vlasenko, V., Stashchuck, N., Hutter, K., 2005. Baroclinic Tides, Theoretical Modeling and Observational Evidence. Cambridge University Press, Cambridge 351pp.

Wunsch, C., Ferrari, R., 2004. Vertical mixing, energy, and the general circulation of the oceans. Annu. Rev. Fluid Mech. 36, 281–314.

Xing, J., Davies, A.M., 1997. The influence of wind effects upon internal tides in shelf edge regions. J. Phys. Oceanogr. 27, 2100–2125.

Xing, J., Davies, A.M., 1999. The influence of topographic features and density variations upon the internal tides in shelf edge regions. Int. J. Numer. Meth. Fl. 31, 535–577.